Inflammation Research (2026) 75:33
https://doi.org/10.1007/s00011-026-02192-y

Inflammation Research

RESEARCH

Spatial transcriptomics identifies IL-32 as a lipid droplet-associated cytokine linked to tubular injury in human diabetic kidney disease

Kieran Meadows[1] · Hyunjae Chung[1] · Son Vo[2] · Aysa Imanzadeh[1] · Heewon Seo[3] · Sisay Getie Belay[1] · Asha Swamy[1] · Wulin Teo[4] · Kevin Chapman[5] · Graciela Andonegui[1] · Hallgrimur Benediktsson[5] · Peter K. Stys[4] · Thang Pham[2] · Daniel A. Muruve[1] · Justin Chun[1]

Received: 3 November 2025 / Revised: 1 January 2026 / Accepted: 18 January 2026

Abstract

Background Diabetic kidney disease (DKD) is a severe complication of diabetes mellitus and the leading cause of chronic kidney disease worldwide. Among the many drivers of tubular injury, lipid accumulation and inflammation are emerging as major contributors to kidney disease progression, but the molecular link between lipid metabolism and inflammatory signaling remains to be determined.

Methods Kidney biopsies from patients with DKD across pathologic classes were labelled for lipid droplets and analyzed by Nile Red spectroscopy. Digital spatial profiling and single-cell spatial transcriptomics were performed on samples from 14 patients representing different DKD classes. RNA scope and immunofluorescence microscopy were used for data validation and characterization.

Results Lipid droplets (LD) were increasingly abundant in advanced stages of DKD, primarily accumulating in the proximal tubules. Single-cell spatial transcriptomics identified several genes—*DUSP5*, *AZU1*, *COL9A1*, *HSPB1*, and *IGFBP7*—as highly upregulated in DKD. Remarkably, *IL32*, which encodes a LD-associated cytokine, was highly enriched in injured proximal tubules. Immunofluorescence confirmed IL-32 localization to LDs predominantly within KIM1 positive tubules in moderate to advanced DKD. Furthermore, injured IL-32 expressing tubules were in close proximity to infiltrating neutrophils and macrophages, immune effectors of non-resolving inflammation and kidney disease progression.

Conclusion IL-32 is a LD-associated cytokine upregulated during tubular injury that represents a potential link between lipid dysregulation, inflammation and progression in human DKD.

Keywords Spatial transcriptomics · Diabetic kidney disease · IL-32 · Tubular injury · Macrophage · Renal inflammation

Introduction

Diabetic kidney disease (DKD) is a major complication of diabetes mellitus and the leading cause of chronic kidney disease (CKD) and kidney failure [1]. The pathogenesis of DKD is complex with multifactorial involvement of metabolic, inflammatory, oxidative stress, hemodynamic, genetic and environmental factors [2]. The histopathologic changes in the kidney associated with diabetes include glomerular basement membrane thickening and mesangial expansion in early DKD and nodular sclerosis (Kimmelstiel-Wilson lesions) in advanced disease [3–5]. The histopathologic classification for DKD (Renal Pathology Society classification) categorizes DKD into four classes according to glomerular lesions: class I, glomerular basement membrane thickening; class II, mesangial expansion; class III, nodular sclerosis;

Communicated by Casimiro Gerarduzzi

✉ Justin Chun
chuj@ucalgary.ca

[1] Department of Medicine, Health Research Innovation Centre 4A12, Snyder Institute for Chronic Diseases, Cumming School of Medicine, University of Calgary, 3280 Hospital Drive NW, Calgary, AB T2N 4Z6, Canada

[2] BioTuring, 4445 Eastgate Mall, San Diego, CA 92121, USA

[3] Snyder Institute for Chronic Diseases, Cumming School of Medicine, University of Calgary, Calgary, AB, Canada

[4] Department of Clinical Neurosciences, Hotchkiss Brain Institute, Cumming School of Medicine, University of Calgary, Calgary, AB, Canada

[5] Department of Pathology and Laboratory Medicine, Snyder Institute for Chronic Diseases, Cumming School of Medicine, University of Calgary, Calgary, AB, Canada

Published online: 07 February 2026

and class IV, advanced diabetic glomerulosclerosis with more than 50% global glomerulosclerosis [6]. Although injury to glomerular endothelial cells and podocytes is associated with albuminuria and reduced glomerular filtration rate [7], there is growing evidence that metabolic, oxidative and pro-inflammatory mediators in proximal tubular cells play important roles in DKD progression [8].

Cellular lipid accumulation has been described in kidney biopsies of DKD patients and is associated with altered lipid metabolism, inflammation and disease severity in DKD, a spectrum referred to as lipotoxicity [9–12]. However, the mechanisms by which lipotoxicity contributes to tubular cell injury, inflammation and kidney disease progression remain poorly understood [13]. Lipid droplets (LD), historically thought to be inert cytoplasmic structures for lipid storage, accumulate in podocytes, mesangial cells and tubular epithelial cells in DKD [10, 14]. More recently, LD are being recognized as important compartments that alleviate cellular stress and regulate energy homeostasis [15]. Tubular epithelial cells, for example, rely on fatty acids as a primary energy source for mitochondrial function, which is essential for fatty acid oxidation [16, 17]. By contrast, excessive buildup of free fatty acids, which can be stored as neutral LD, is associated with cellular dysfunction and lipotoxicity [18]. In experimental diabetes models, renal accumulation of triglycerides and cholesterol contributes to the expression of profibrotic growth factors and pro-inflammatory cytokines, increases oxidative stress, and promotes key features of diabetic kidney disease (DKD), including glomerulosclerosis, tubulointerstitial fibrosis, and proteinuria [19–21]. In podocytes, both lipid accumulation and the species of lipids, such as sphingomyelin phosphodiesterase acid-like 3b, cholesterol, or palmitic acid, correlate with or induce inflammatory gene expression, oxidative stress, endoplasmic reticulum stress, and/or mitochondrial dysregulation in vitro, pathways that contribute to the pathogenesis of DKD [22–24]. ATP-binding cassette transporter 1 (ABCA1) and vascular endothelial growth factor B (VEGF-B) have been found to be associated with lipid droplet accumulation, renal lipotoxicity, and impaired kidney function [25–28]. In the tubular epithelium, lipotoxicity can drive cellular injury that includes mitochondrial dysfunction, apoptosis, tubular atrophy, and tubulointerstitial fibrosis [29]. In this regard, Mori et al. demonstrated that targeting kidney injury molecule 1 (KIM-1) mediated tubular cell uptake of fatty acids could ameliorate inflammation and fibrosis and delay experimental DKD progression [30]. Therefore, while there appears to be a clear association between lipid accumulation, lipotoxicity and DKD pathogenesis, the molecular pathways linking lipids to cellular injury and dysfunction in the kidney have been largely unexplored.

In this study, we used a combination of Nile Red spectroscopy, immunofluorescence microscopy, digital spatial profiling and single-cell spatial transcriptomics of kidney biopsies to characterize lipid accumulation and its associated molecular signature in human DKD. We identified IL-32 as a human-specific, pro-inflammatory cytokine that is upregulated in DKD and localized specifically to LD primarily in injured proximal tubular cells. Injured proximal tubules expressing *HAVCR1* (encoding KIM-1) and *IL32* were found in close proximity to infiltrating macrophages and neutrophils that are known to drive chronic non-resolving renal inflammation and disease progression [31]. Collectively, these data suggest that LD-associated IL-32 may represent an important mediator of lipotoxicity linking lipid accumulation, tubular injury and inflammation in the pathogenesis of human DKD.

Methods

Human nephrectomy and kidney biopsy samples

All experiments involving human samples were approved by the Conjoint Health Research Ethics Board at the University of Calgary. Human kidney biopsies from control and patients with diabetic kidney diseases were obtained from the Biobank for the Molecular Classification of Kidney Disease, Calgary, AB, Canada (REB20-1999). Non-diseased segments of nephrectomy samples were obtained from patients with renal cell carcinoma (REB15-1158). Demographic and clinical data for patients are summarized in Supplementary Tables 1 and 2.

Nile red staining and fluorescence spectroscopy of kidney biopsy samples

Frozen control or DKD patient kidney biopsies were cryosectioned at 40 µm thickness on a glass slide and fixed in 4% paraformaldehyde (PFA). Sections with stained with 14 µM Nile Red (Sigma, #72485). A LSM 880 microscope (Zeiss) was used to capture fluorescence spectral data with 488 nm laser to acquire spectral fluorescence images ranging from 494 to 691 nm for three to five fields of view that include glomeruli or tubules.

Immunofluorescence of formalin-fixed paraffin-embedded kidney sections

Standard deparaffinization and immunofluorescence procedures were performed on formalin-fixed paraffin-embedded (FFPE) tissue sections from control and DKD patients. After deparaffinization and rehydration through a graded

EtOH series, antigen retrieval was performed using boiling citrate buffer solution (pH = 6.0) from DAKO (#S169984-2) in a steamer for 20 min. Tissue sections were then blocked in blocking buffer (1% BSA, 2% donkey serum in PBS) for 1 h at room temperature, followed by incubation with primary antibodies including anti-PLIN2 (1:200, R&D Systems, #MAB76341), anti-KIM-1/HAVCR1 (1:100, R&D Systems, #MAB1750), anti-NPHS1 (1:100, R&D Systems, #AF4269), anti-ACE-2 (1:200, R&D Systems, AF933), anti-IL-32 (1:200, Proteintech, # 11079–1-AP), and anti-CD68 (1:100, Invitrogen, MA5-13324) in blocking buffer at 4 °C overnight. After three PBS washes for 5 min each, tissue sections were incubated with fluorescent-dye-conjugated secondary antibodies and fluorescein-conjugated lotus tetragonolobus lectin (LTL-FITC; 1:100, Vector Laboratories, Cat. #FL-1321–2) in blocking buffer for 1 h at room temperature. After three PBS washes, tissue sections were mounted with ProLong Gold antifade mounting medium with or without Hoescht 33342 (1:1000, Sigma, #14,533). Confocal images were acquired using an LSM 880 (Zeiss) or a FV4000 (Olympus) confocal microscope.

GeoMx digital spatial profiling

Two sets of slides containing 5 µm serially sectioned tissue samples from 2 FFPE transplant control pre-implantation biopsies and 3 DKD (class III) biopsies were prepared. Digital spatial RNA profiling was performed on one set using the NanoString GeoMx Digital Spatial Profiler (DSP) [32] following the NanoString GeoMx DSP slide preparation (MAN-10150) and NGS readout (MAN-10153) manual. The slides for GeoMx were prepared by baking in a drying oven at 60 °C for 1 h and processed using the Leica BOND platform (Leica Biosystems). Briefly, deparaffinization was performed with CitriSolv, followed by rehydration through a graded ethanol series. Targets were exposed by incubating with 1X Tris–EDTA buffer (pH 9), followed by 1 µg/ml proteinase K digestion. Next, Human Whole Transcriptome Atlas (WTA) Probes (NanoString Technologies) were hybridized to the tissues at 37°C overnight. Excess and off-target probes were removed by 2 × saline sodium citrate (2 × SSC)/50% formamide. After washing, the slides were blocked in Buffer W and stained with morphological markers for 1 h at room temperature. The fluorescent conjugated morphology markers used are CD10 (1:10, Abcam, #ab261729), PanCK (1:10, NanoString, #121301310) and SYTO 13 nucleic acid stain (1:10, NanoString, #121300310). Excess markers were removed with two washes in 2 × SSC. Stained slides were loaded onto a GeoMx Digital Spatial Profiler, and the entire core biopsies were scanned. The other FFPE serially sectioned biopsy tissue samples underwent deparaffinization, antigen retrieval and immunostaining with KIM1 antibody and LTL-FITC using a standard immunofluorescence protocol. Subsequently, confocal images were taken to identify non-injured (LTL+, KIM1-) vs injured (KIM1+) proximal tubules in each biopsy sample. 6–14 areas of interest (AOI) were selected from each biopsy, including 3–8 glomeruli and 3–6 proximal tubules (KIM1- or KIM1+), guided with the morphological markers (CD10, PanCK) and the serially sectioned tissues stained with KIM1 and LTL-FITC (Supplementary Fig. 1). RNA-ID and UMI-containing oligonucleotide tags were UV-cleaved from the WTA panel within the chosen ROIs collected in a 96-well collection plate. For library preparation, Illumina i5 and i7 dual indexing primers were added to the oligonucleotide tags during PCR to index each area of illumination (AOI) uniquely. AMPure XP beads (Beckman Coulter) were used for PCR purification. Library concentration was measured using a Qubit fluorometer (Thermo Fisher Scientific), and quality was assessed using a Bioanalyzer (Agilent Technologies). Sequencing was performed on an Illumina NextSeq 2000 (Illumina Inc.), and FASTQ files were processed into gene count data for each sample using the GeoMx® NGS Pipeline. Read depth was performed with total transcripts identified across nuclei, corresponding to an average of transcripts per nucleus.

RNAscope-IHC

In situ Hybridization was performed to detect *IL32* mRNA in control and DKD patient kidney FFPE tissue sections using IL-32 RNAscope probe and multiplex fluorescent V2 assay kit (Advanced Cell Diagnostics, #323100) according to the manufacturer's protocol. Briefly, tissue sections of 4 µm thickness were deparaffinized, washed with EtOH and peroxidase-blocked. Antigen retrieval was performed for 15 min in a steamer, followed by protease digestion using reagents provided by the kit. The IL-32 (Advanced Cell Diagnostics, #541431-C2) or negative control DapB (Advanced Cell Diagnostics, #310,043) RNAscope probe was incubated with the tissue at 40°C in a HybEZ hybridization oven (Advanced Cell Diagnostics) for 2 h, followed by Opal 570 dye (Akoya Biosciences, #FP1488001KT) incubation for 30 min. Subsequently, a standard immunofluorescence procedure was performed to label proximal tubular cells with anti-SGLT2 antibody (1:100, Proteintech, #24654–1-AP). Tissue sections were mounted with Prolong Gold antifade mounting medium containing DAPI (Invitrogen, #P36931).

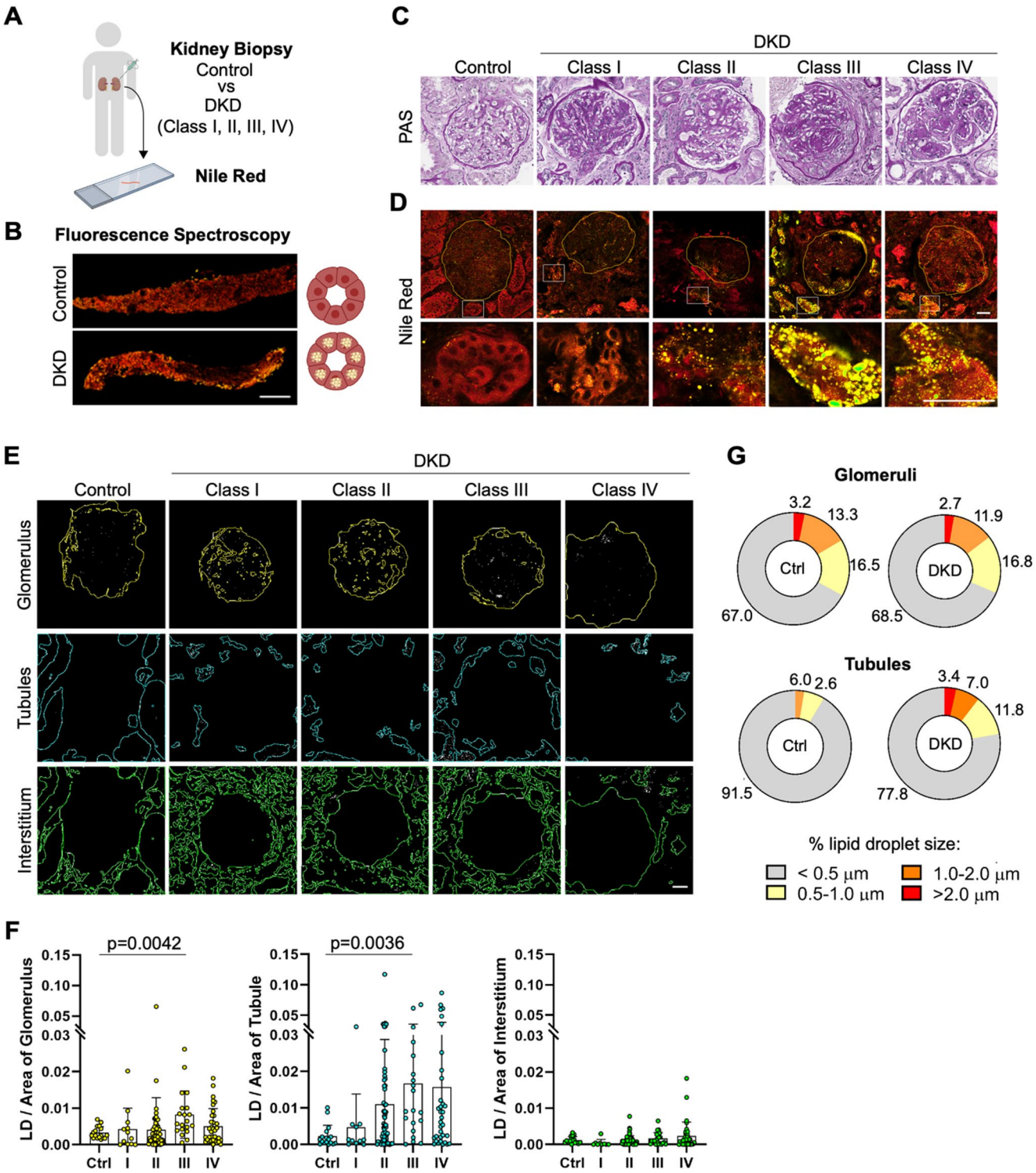

Fig. 1 Upregulation of lipid droplets in DKD kidney biopsies. **A** Experimental design for Nile Red staining of frozen kidney biopsies from control and patients with class I-IV DKD, **B** Nile Red fluorescence images showing lipid droplets (LDs) in kidney biopsies of control and DKD patients. Scale bar, 1 mm, **C** Periodic Acid- Schiff (PAS) stained kidney biopsies from control and patients with classes I-IV DKD, **D** Nile Red-stained kidney biopsies from control and patient with classes I-IV DKD. Lower panels: magnified views of boxed areas with LDs in tubules; yellow lines mark glomeruli. Scale bar, 20 µm, **E** Automated segmentation of glomeruli (yellow), tubules (blue), and interstitium (green) in Nile red-stained images from control and DKD biopsies. Scale bar, 20 µm, **F** Quantification of LDs in segmented glomeruli, tubules, and interstitium from control (n = 5) and DKD (class I, n = 3; class II, III, IV, n = 10 each) biopsies. Data are mean ± SD; unpaired Student's t-test at the indicated p-values, **G** LD size distribution in glomeruli and tubules in control (n = 5) and DKD (class III, n = 10) biopsies.

Spatial transcriptome (pre)processing, DE analysis and enrichment test

NanoString GeoMx DSP (Digital Spatial Profiler) outputs a raw count matrix, and we followed the recommended filtering and normalization steps, including upper-quartile (UQ) normalization using the R package GeomxTools (v3.4.0). Then, variance stabilization normalization (VSN) was applied to the UQ matrix using the R package vsn (v3.68.0) to stabilize the variance to make genes comparable. Differential expression (DE) analysis between the groups of interest was carried out using the R (v4.3.1) t.test built-in function with the var.equal = FALSE parameter. DE genes were selected when the FDR value was less than 0.05 and the absolute value of the Log2 fold-change was greater than 0.30. The volcano and box plots were generated using the R package ggplot2 (3.4.4), ggrepel (v0.9.4), and ggpubr (v0.6.0).

CosMx molecular spatial imaging processing

Formalin-fixed, paraffin-embedded samples were prepared according to the manufacturer's specifications (NanoString Technologies). As we previously described [33], tissue sections were cut at 5 µm thickness using a Leica microtome onto Leica BOND PLUS slides (Leica Biosystems, S21.2113.A). Through a collaboration with the NanoString CosMx spatial molecular imager (SMI) Technology Access Program, a 1000-plex CosMx Human Technology Access Program (TAP) RNA panel was performed with the addition of kidney-specific custom genes: *APOL1, AQP1, AQP2, CLDN10, EMCN, HAVCR1, LRP2, NOS1, NPHS1, PALMD, PIEZO2, PLVAP, PROM1, PROX1, REN, SCN2A, SH3GL3, SLC12A1, SLC12A3, SLC14A2, SLC26A4, SLC26A7, SLC4A9, SLC5A12, SLC5A2, SLC7A13, SLC8A1, SYN1, UNC5D*. Morphology visualization for upfront staining was performed using CD298, B2M, PanCK, CD45, and/or CD68 and DAPI and post-staining with CD10 and podoplanin.

CosMx data preprocessing, cell type annotation, and neighborhood analysis

We followed the analytical workflow described in Vo et al. [33]. Briefly, we utilized the original cell segmentation provided by NanoString, which was subsequently dilated by 10 pixels or until adjacent boundaries were reached. Transcripts were then assigned to individual cells to generate a cell-by-gene expression matrix. Cells having fewer than 20 total transcript counts were excluded from downstream analyses. CosMx quality control metrics are displayed in Supplementary Fig. 2. Transcript counts between cells were normalized by dividing by the segmented cell area (in pixels) and then rescaled by multiplying by the mean area across all cells, thereby preserving the overall count magnitude. Finally, we applied a natural log-transformation to all expression values.

Batch correction across samples was performed using single-cell Variational Inference (SCVI) [34]. The SCVI latent embedding was used to construct a UMAP representation (n_neighbors = 50) followed by Leiden clustering [35]. Clusters were manually assigned to known kidney cell types based on canonical marker gene expression. For neighborhood analysis, spatial coordinates were converted into physical units (µm) by scaling pixel coordinates according to the FOV's actual dimensions (512 × 512 µm). For each cell, neighboring populations were defined within a radius of 100 µm, 70 µm, 50 µm, and 30 µm using NearestNeighbors from scikit-learn with the "kd_tree" algorithm [36]. Statistical comparisons between cell populations were conducted using the Wilcoxon rank-sum test. Analysis and figures were generated using the BioTuring Lens platform.

Active and chronic tissue scoring

Whole biopsy histology stain images were acquired for class II and class III DKD tissue. For active and chronic disease phenotypes, areas of interest were selected based on immune cell infiltration, collagen deposition, tubular atrophy, tubular injury marker expression (*HAVCR1*), and changes in the populations of fibroblasts and myofibroblasts. Immune cell infiltration was assessed using H&E staining, where regions of interest were thresholded and analyzed for increased nuclei density and size (Supplementary Fig. 3). Collagen deposition, assessed by Masson Trichrome staining, were thresholded and quantified for the percentage of the region of interest area that was positive for collagen deposition (Supplementary Fig. 3). The chronic disease phenotype was defined as tissue regions with more than 5 nuclei per 1000 μm^2 and greater than 10% area coverage of collagen deposition. Active phenotype regions were defined by the presence of injured proximal tubular cells, while chronic regions showed a loss of organization, atrophy of proximal tubular cells and regions of increased fibroblast and myofibroblast cell types.

Quantification and statistical analyses

Data are presented as mean ± standard deviation (SD) unless stated otherwise in the legends. Unpaired Student's t-test or one-way ANOVA with Tukey's post hoc test were applied for pairwise comparisons or multiple comparison test, respectively. Graph Pad Prism v10 was used to perform statistical analyses. A *p*-value of less than 0.05 was considered

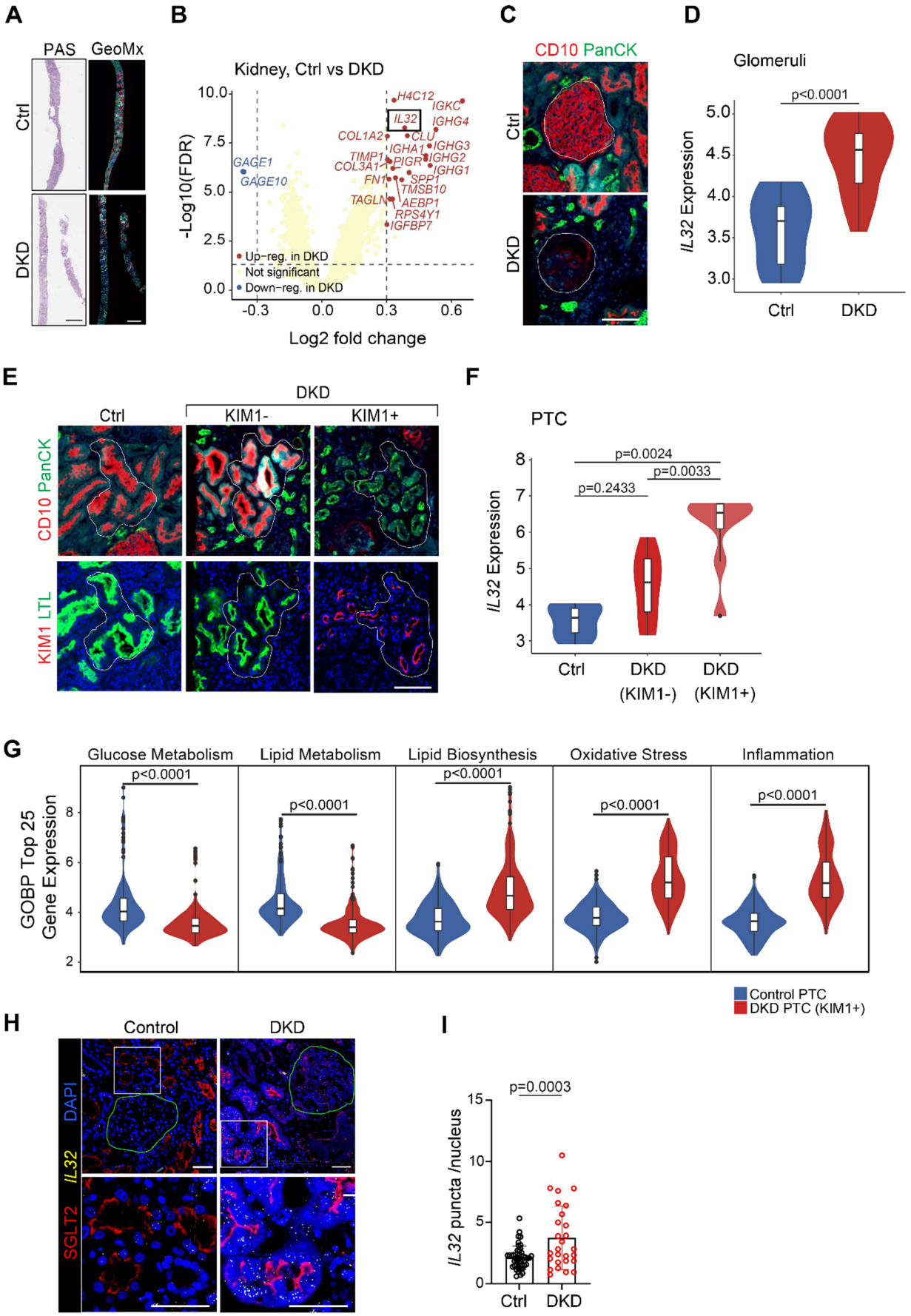
A
PAS
GeoMx
Ctrl
DKD
B
Kidney, Ctrl vs DKD
-Log10(FDR)
Log2 fold change
Up−reg. in DKD
Not significant
Down−reg. in DKD
H4C12
IGKC
IL32
IGHG4
COL1A2
CLU
IGHA1
IGHG3
TIMP1
PIGR
IGHG2
COL3A1
IGHG1
GAGE1
GAGE10
FN1
SPP1
TMSB10
TAGLN
AEBP1
RPS4Y1
IGFBP7
C
CD10 PanCK
Ctrl
DKD
D
Glomeruli
p<0.0001
IL32 Expression
Ctrl
DKD
E
DKD
Ctrl
KIM1-
KIM1+
CD10 PanCK
KIM1 LTL
F
PTC
p=0.0024
p=0.0033
p=0.2433
IL32 Expression
Ctrl
DKD (KIM1-)
DKD (KIM1+)
G
Glucose Metabolism
Lipid Metabolism
Lipid Biosynthesis
Oxidative Stress
Inflammation
p<0.0001
GOBP Top 25 Gene Expression
Control PTC
DKD PTC (KIM1+)
H
Control
DKD
DAPI
IL32
SGLT2
I
p=0.0003
IL32 puncta /nucleus
Ctrl
DKD

Fig. 2 IL-32 is upregulated in glomeruli and proximal tubules of DKD. **A** Periodic Acid-Schiff (PAS) stained and immunofluorescence images from control or DKD biopsies for analysis by GeoMx. Scale bar, 100 µm, **B** Volcano plot of differential gene expression between DKD (red) and control (blue) groups, **C** Immunofluorescence of control and DKD biopsies labelled with CD10 (red) and PanCK (green). Scale bar, 100 µm, **D** Boxplots of IL-32 mRNA expression in glomeruli among control and DKD biopsies, **E** Immunofluorescence images of FFPE kidney tissues stained for CD10 (red), PanCK (green) or KIM1 (red) or LTL (green). Scale bar, 100 µm, **F** Boxplots of IL-32 mRNA expression in proximal tubules among control and DKD biopsies, **G** Boxplots of top 25 leading genes from GSEA in control proximal tubules (blue) and diabetic KIM1+injured proximal tubules (red), **H** RNAscope for IL-32 mRNA (yellow) and co-immunofluorescence for SGLT2 (red) in control and DKD kidney biopsies; outlined glomerular regions shown. Scale bar, 20 µm, **I** Analysis of IL-32 mRNA puncta in tubular regions of kidney biopsies (n = 27-46). Data are mean ± SD; Student's t-test, $p = 0.0003$.

significant. The immunoblot, RNAscope and immunofluorescence images are representative of multiple biopsies.

Data availability

GeoMx and CosMx datasets generated in this study will be made available at the NCBI's Gene Expression Omnibus (GEO, https://www.ncbi.nlm.nih.gov/geo/) prior to publication. All analyses were performed using publicly available software or BioTuring Lens as described in the Methods section. Processed datasets will be made available for reanalysis upon request.

Results

Increased lipid droplets in diabetic kidney disease

In human diabetic kidney tissue, LD are found in abundance in podocytes, mesangial cells and proximal tubules [10]. To examine the correlation between LD and kidney injury, we first evaluated LD abundance in deidentified human kidney biopsies from controls (normal margins of nephrectomy tissue, n = 5) and patients with diabetic kidney disease (total; n = 33; class I, n = 3 and classes II-IV, n = 10 for each) using fluorescence microscopy and Nile Red to label lipid droplets [37] (Fig. 1A, B). LD size, distribution, and quantity were determined using a machine learning-based semi-auto segmentation algorithm as we previously described [38], and correlated with the Renal Pathology Society DKD classification based on conventional histopathology using Periodic Acid-Schiff (PAS) stain (Fig. 1C). The number of detectable LD increased from class I to III in glomeruli parallel with injury, followed by a decline in the number for class IV DKD, presumably due to advanced glomerulosclerosis (Fig. 1D–F). Interestingly, LD accumulation in tubules peaked in class III DKD and remained persistently elevated in class IV DKD (Fig. 1F). Moreover, while the distribution of LD size was similar in the glomeruli across the biopsies, there was a shift towards larger LD size (1.0 to > 2.0 µm) in the tubules of DKD patients compared to control kidneys (Fig. 1G). These results show that LD abundance correlates with pathologic severity of DKD, with most LD changes occurring in the tubular cell compartment.

Identification of IL-32, a lipid droplet-associated protein in DKD

The abundance of lipid droplets in advanced DKD led us to hypothesize that there may be lipid droplet-associated genes upregulated with tubular injury and involved in the pathogenesis of DKD. To determine potential candidates, we used NanoString's Digital Spatial Profiling GeoMx platform in healthy control tissue from pre-transplantation biopsies and kidney biopsies from patients with biopsy-proven DKD. In both control kidney and DKD biopsies, three glomerular regions of interest (ROI) and five proximal tubular ROI were selected to undergo transcriptomic analysis in ROIs using the NanoString Digital Space Profiling GeoMx platform (Fig. 2A, Supplementary Fig. 1). Differential expression of genes was determined using a false discovery rate (FDR) threshold of < 0.05 and an absolute value of the Log2 fold-change > 0.30. Amongst the highest upregulated genes, DKD kidney biopsies included *H4C12*, *IGKC*, *IGHG4*, *IL32* and *CLU* (Fig. 2B). Among the candidate genes, we focused on *IL32* (encoding interleukin 32), as it has been previously suggested as a potential lipid droplet-associated protein expressed in the serum of diabetic patients [39, 40]. We compared uninjured glomeruli with preserved architecture from control samples to sclerosed glomeruli from DKD tissue (Fig. 2C). Spatial analysis of glomeruli of DKD patients indeed showed upregulation of *IL32* in the glomeruli (Fig. 2D). Next, we examined *IL32* expression in proximal tubules that were either uninjured (as identified by kidney injury molecule negative; KIM1-) or injured (KIM1+). Compared to KIM1- tubules, injured KIM1+tubules demonstrated a significant upregulation of *IL32* (Fig. 2F). Comparison of the top 25 genes per biological process between KIM1- tubules and injured KIM1+tubules found significant downregulation of glucose and lipid metabolism, while lipid biosynthesis, oxidative stress and inflammation were significantly upregulated in injured tubules (Fig. 2G). RNA scope was used to confirm the *IL32* expression in injured proximal tubules as identified by SGLT2, which showed significantly higher IL32 expression in DKD proximal tubules compared to control (3.74 vs 2.14, p-value = 0.0003) (Fig. 2H and I).

IL-32 protein expression was next explored in human kidney biopsies from the different classes of DKD and healthy controls. IL-32 expression was hardly detectable

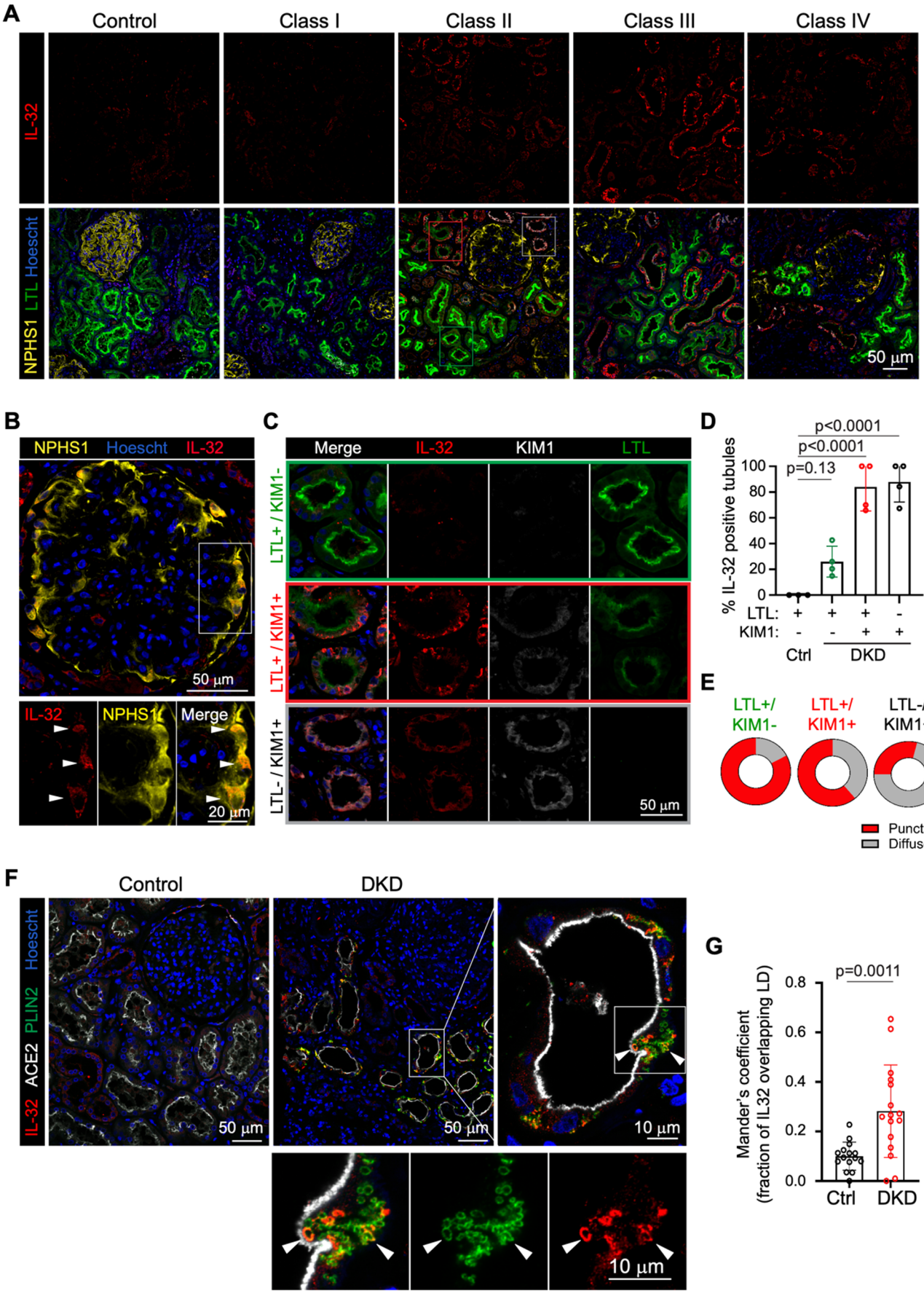
A
Control
Class I
Class II
Class III
Class IV
IL-32
NPHS1 LTL Hoescht
50 µm
B
NPHS1 Hoescht IL-32
50 µm
IL-32
NPHS1
Merge
20 µm
C
Merge
IL-32
KIM1
LTL
LTL+ / KIM1-
LTL+ / KIM1+
LTL- / KIM1+
50 µm
D
p<0.0001
p<0.0001
p=0.13
% IL-32 positive tubules
100
80
60
40
20
0
LTL: + + + -
KIM1: - - + +
Ctrl
DKD
E
LTL+/ KIM1-
LTL+/ KIM1+
LTL-/ KIM1+
Punctate
Diffuse
F
Control
DKD
IL-32 ACE2 PLIN2 Hoescht
50 µm
50 µm
10 µm
10 µm
G
p=0.0011
Mander's coefficient (fraction of IL32 overlapping LD)
0.8
0.6
0.4
0.2
0.0
Ctrl
DKD

Fig. 3 IL-32 expression in proximal tubules at lipid droplets precedes injured proximal tubules highly expressing KIM1. **A** Confocal images from FFPE control and DKD (classes I- IV) kidney tissues showing IL-32 (red), NPHS1 (yellow), LTL (green) with Hoescht to label nuclei. Scale bar, 50 µm, **B** Representative glomeruli from DKD patient (class II from panel A) with magnified regions (white outline) and arrowheads showing regions of IL-32 colocalization with NPHS1, **C** Tubular regions outlined in green (LTL+/KIM1-), red (LTL+/KIM1+) and white (LTL-/KIM1+) for Class II DKD from panel 3A. Individual channels including KIM1 (white). Scale bars as indicated, **D** Quantification of tubules for IL-32 expression in control patients (n = 3) and DKD patients (n = 4) in LTL+/KIM1- (green), LTL+/KIM1+ (red) and LTL-/KIM1+ (black outline) tubules, **E** Quantification of the proportion of tubular regions exhibiting a punctate (red) or diffuse (grey) pattern of IL-32 distribution, **F** Confocal images of healthy control or DKD (class III) showing colocalization of IL-32 (red) with PLIN2 (green) in proximal tubules labelled by ACE2. Arrowheads in inset shows regions of IL-32 colocalization with PLIN2., PLIN2 (green); Hoescht (blue) stains nuclei. Scale bar, 50 µm, **G** Quantification of IL-32 and PLIN2 colocalization in control and DKD tissues (n = 15-16). Data are mean ± SD; Student's t-test, p = 0.0011.

in control and class I DKD, but abundant in DKD classes II to IV (Fig. 3A). Interestingly the highest expression of IL-32 occurred in cells weakly positive for lotus tetragonolobus lectin (LTL), a phenotypic marker of proximal tubules (Fig. 3A). High resolution micrographs of glomeruli confirmed some IL-32 expression in nephrin-positive podocytes but was not readily detectable in most patient biopsy samples (Fig. 3B). In contrast, we observed varying degrees of IL-32 expression in the proximal tubules of DKD patients (Fig. 3C). Healthy proximal tubules with high LTL signal (LTL+/KIM1-) had minimal expression of IL-32, while regions of lower LTL expression had some expression of KIM1 (LTL+/KIM1+) and high levels of IL-32 expression in a punctate pattern (Fig. 3C and D). In injured proximal tubules highly expressing KIM1 (LTL-/KIM1+), IL-32 localization was more diffuse. Quantification of proximal tubules expressing punctate or diffuse IL-32 location showed 70% IL-32 puncta in LTL+/KIM1-, 58% IL-32 puncta in LTL+/KIM1+ and 29% IL-32 puncta in LTL-/KIM1+ (Fig. 3E). Interestingly, the fraction puncta pattern was highest in the LTL+/KIM1- proximal tubules, suggesting that the localization of IL-32 to lipid droplets precedes redistribution of IL-32 to more diffuse structures. To confirm that the punctate structures to which IL-32 was localized were LDs, we co-stained IL-32 with the lipid droplet marker perilipin 2 (PLIN2) (Fig. 3F). Indeed, we observed a higher fraction of PLIN2 signal overlapping with IL-32 and increased LD size in DKD compared (mean Mander coefficient 0.28) to control tissue (mean 0.10; $p = 0.0011$) (Fig. 3F and 3G), suggesting a stronger association of IL-32 with enlarged lipid droplets in the disease state. Taken together, these show that IL-32 is an intracellular LD-associated cytokine that increases primarily in injured proximal tubules in human DKD.

Spatial transcriptomics identifies IL32 as a DKD gene-of-interest

To further analyze the molecular signatures across a breadth of human DKD tissue samples, NanoString's CosMx single-cell digital spatial transcriptomics was employed on full-length kidney biopsy core tissues. Tissue samples from a total of 17 different patient biopsies, ranging from non-DKD control to class IV DKD, were sectioned and analyzed (Fig. 4A). Cell typing was completed, resulting in the annotation of 16 distinct cell clusters, including proximal tubule, podocyte, endothelial, distal tubule, and other resident kidney populations, as well as macrophage, neutrophil, B cell, and T cell immune populations (Fig. 4B, C). By comparing the cell compositions across DKD classes, a decrease in podocytes and healthy proximal tubules from 3.2% to 0.8% and 23.4% to as low as 11.5% can be seen, respectively, as well as an increase in T and B cells from 2.5% to 7.8% and 2.1% up to 6.0% respectively (Fig. 4D). The injured proximal tubule population was distinguished from the healthy proximal tubule population by the expression of *HAVCR1* encoding for KIM1. Differential expression of genes was then computed between all cell populations in diabetic tissue compared to control for genes with an adjusted *P*-value < 0.05 (Fig. 4E). Amongst the highest upregulated genes identified by CosMx were *DUSP5, NPPC, AZU1, COL9A2, HLA-DPA1,* and *VIM* (Fig. 4E). By cross-referencing the CosMx differential expression data with GeoMx, *IGKC, IL32,* and *CLU* were also identified (Fig. 4E). When comparing the differential expression of each DKD class to control, *IL32* consistently appeared among the top 25 differentially expressed genes (DEG) and was among the top 10 genes found to be upregulated in each class (Supplementary Fig. 4). The top DEGs were visualized using a heatmap and dot plot to analyze cell type specificity (Fig. 4F, G). Genes such as *DUSP5*, *NPPC*, and *VIM* showed increased expression in the endothelial, proximal tubule, and podocyte populations, while changes in *IL32* expression were specific to the proximal tubule cells (Fig. 4F). Up to 50% of proximal tubular cells expressed *IL32* with minimal differences in *IL32* expression occurring in endothelial and podocyte populations (Fig. 4G). These results are consistent with previous transcriptomic and immunofluorescence data, confirming that *IL32* expression is primarily increased in the proximal tubules of human DKD.

Tubular injury correlates with IL32 expression in DKD

Given the predominant changes in *IL32* expression observed in the proximal tubular cells in the kidney biopsies of DKD patients, single-cell digital spatial transcriptomic data were

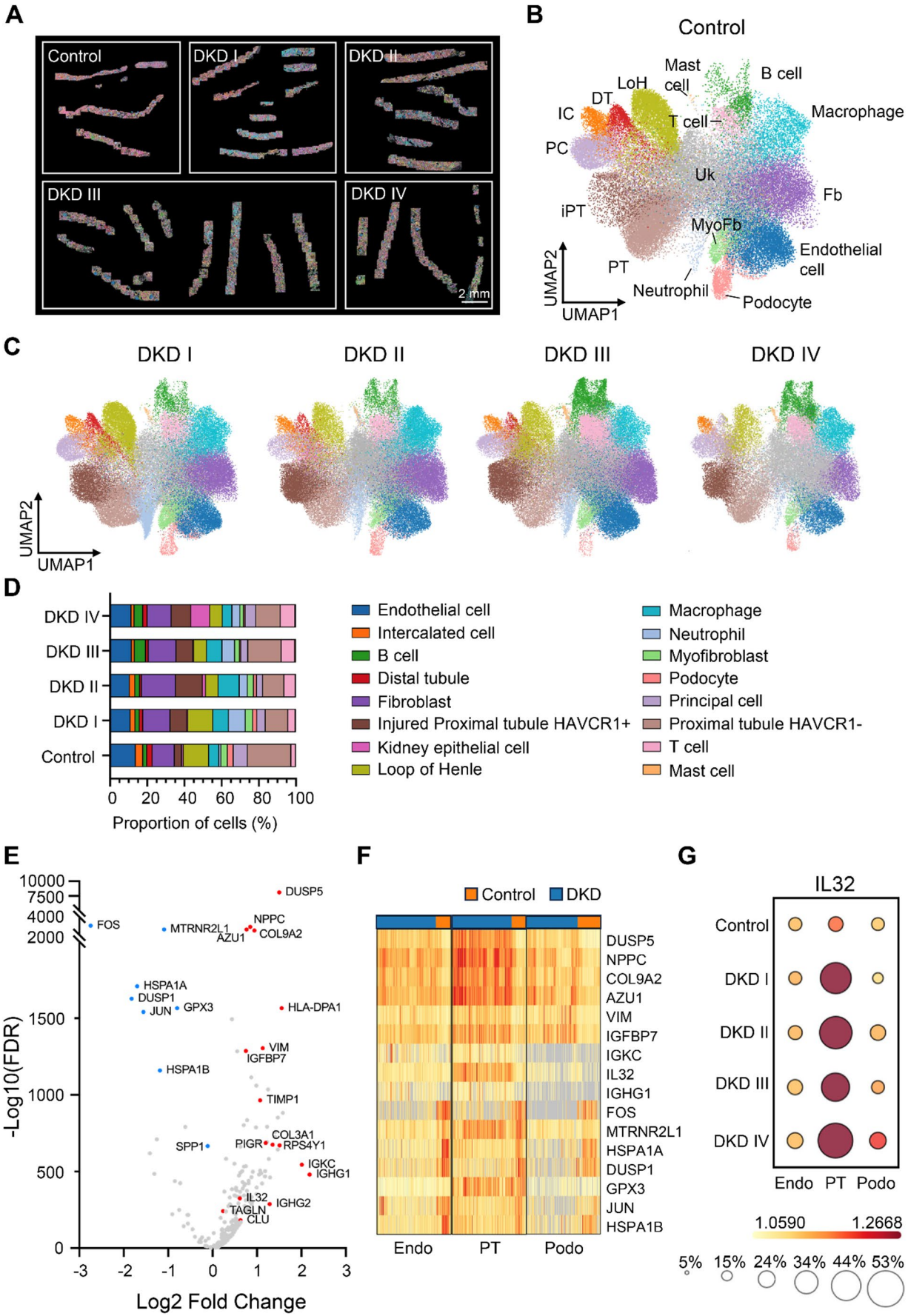
A
Control
DKD I
DKD II
DKD III
DKD IV
2 mm
B
Control
Mast cell
B cell
LoH
DT
IC
T cell
Macrophage
PC
Uk
Fb
iPT
MyoFb
Endothelial cell
PT
Neutrophil
Podocyte
UMAP2
UMAP1
C
DKD I
DKD II
DKD III
DKD IV
UMAP2
UMAP1
D
DKD IV
DKD III
DKD II
DKD I
Control
0 20 40 60 80 100
Proportion of cells (%)
Endothelial cell
Intercalated cell
B cell
Distal tubule
Fibroblast
Injured Proximal tubule HAVCR1+
Kidney epithelial cell
Loop of Henle
Macrophage
Neutrophil
Myofibroblast
Podocyte
Principal cell
Proximal tubule HAVCR1-
T cell
Mast cell
E
-Log10(FDR)
Log2 Fold Change
DUSP5
FOS
MTRNR2L1
NPPC
AZU1
COL9A2
HSPA1A
DUSP1
JUN
GPX3
HLA-DPA1
VIM
IGFBP7
HSPA1B
TIMP1
COL3A1
SPP1
PIGR
RPS4Y1
IGKC
IGHG1
IL32
IGHG2
TAGLN
CLU
F
Control
DKD
DUSP5
NPPC
COL9A2
AZU1
VIM
IGFBP7
IGKC
IL32
IGHG1
FOS
MTRNR2L1
HSPA1A
DUSP1
GPX3
JUN
HSPA1B
Endo
PT
Podo
G
IL32
Control
DKD I
DKD II
DKD III
DKD IV
Endo PT Podo
1.0590
1.2668
5% 15% 24% 34% 44% 53%

Fig. 4 Cell annotation and differential gene expression analysis of human kidney biopsies analyzed using CosMx spatial transcriptomics. **A** Tissue samples analyzed using CosMx spatial transcriptomics imaging clustered by diabetic kidney disease class, **B** UMAP cell type annotation of healthy control tissue. Fibroblast (Fb), myofibroblast (MyoFb), proximal tubule (PT), injured proximal tubule (iPT), principal cell (PC), intercalated cell (IC), distal tubule (DT), Loop of Henle cell (LoH), and unknown cell (Uk), **C** UMAP cell typing of DKD class I-IV tissue coloured by cell type, **D** Percentage population of annotated cell types present in tissue samples sorted by sample class, **E** Differential gene expression calculation of diabetic tissue compared to control across all cell clusters with key genes of interest cross-referenced with previously shown GeoMx data. DEGs were calculated using a Venice statistical analysis. FDR, false discovery rate, **F** Heatmap of differentially expressed genes split by cell type for endothelial (Endo), proximal tubule (PT), and podocyte (Podo) populations. Blue regions on the top axis denote DKD cells while orange regions denote control tissue, **G** Dotplots of relative changes in IL32 expression in endothelial (Endo), proximal tubule (PT), and podocyte (Podo) populations, split by DKD class.

further interrogated to evaluate the relationship between *IL32* and the expression of tubular injury-associated gene expression. *HAVCR1* (encoding KIM1) was initially used as a proximal tubule injury marker, allowing for the annotation of injured and uninjured proximal tubule populations. By comparing *HAVCR1* and *IL32* expression on UMAPs split by DKD class, we observed increasing *IL32* expression primarily in the injured *HAVCR1*-expressing proximal tubule (iPT) population compared to uninjured *HAVCR1*-negative tubules (Fig. 5A). *IL32* expression levels in healthy proximal tubule and injured proximal tubule cells were compared between DKD classes, and a significant increase in *IL32* expression was found in the injured population compared to healthy proximal tubules across all classes, with expression nearly doubling in diabetic tissue (Fig. 5B). To further corroborate this finding, spatial transcription of *IL32* was visualized in relation to tissue cell typing (Fig. 5C). *IL32* expression in control samples was found to be scattered with low clustering, whereas the DKD classes, particularly class II, showed a strong correlation of *IL32* expression with cells annotated as injured proximal tubules (Fig. 5C and Supplementary Fig. 5). Additionally, increased *IL32* expression was associated with a higher proportion of injured proximal tubule populations within the total tissue in DKD biopsies compared to control (Fig. 5D) and also in cells expressing *VCAM1*, another marker of maladaptive injured tubular cells [41, 42] (Fig. 5E). Notably, the expression of IL32 in injured proximal tubules was striking, as few other inflammatory cytokines, such as *TNF, IL6, IL10, IL18,* and *IL33,* changed substantially between healthy proximal tubules and injured proximal tubules across DKD classes (Fig. 5E). Furthermore, *IL32* expression was not observed above the threshold of healthy proximal tubules in other cell types, particularly macrophages, T cells, B cells or neutrophils (Fig. 5F). Taken together, this data further supports the premise that *IL32* is a prominent cytokine expressed in injured proximal tubular epithelial cells in human DKD.

IL32-expressing proximal tubules exist in pro-inflammatory cellular communities

The previous experiments consistently demonstrated the upregulation of *IL32*, an LD-associated cytokine, in injured proximal tubules at the mRNA and protein level in human DKD. To begin addressing the potential role of IL-32 in DKD pathogenesis, an evaluation of the spatial organization of immune cells and proximal tubules in DKD kidney biopsies was performed. Compared to control biopsies, as expected, total immune cell populations were substantially increased across all DKD classes (9.1% vs 19.9%) that included T-lymphocytes (2% vs 6.4%), B lymphocytes (1.7% vs 4.9%), macrophages (4.5% vs 8.7%), and neutrophils (0.9% vs 7.8%) (Fig. 6A). Due to the limited probe repertoire in the CosMx 1000-plex panel, a detailed interrogation of immune cell subtypes was not possible. Nevertheless, annotated single-cell digital spatial transcriptomic data was segmented into injured and uninjured proximal tubule regions in control and DKD biopsies (Fig. 6B, C). Cells were then assigned a specific label based on their proximity to cell types annotated as proximal tubule and injured proximal tubule, defined as < 30 µm, 30–50 µm, 50–100 µm, and > 100 µm calculated from cell center to the nearest uninjured proximal tubule and injured proximal tubule (Fig. 6D). Next, we compared the proportion of each cell type in proximity to injured proximal tubule labelled cells (Fig. 6E). From the composition plot, the T cell proportion remained constant across the distance groups, while the B cells and neutrophils showed a trend of increasing distance from injured proximal tubular cells (Fig. 6E, Supplementary Fig. 6). In contrast, macrophages were in closer proximity to injured proximal tubules (Fig. 6E, F). A significantly higher proportion of macrophages (13.1%) was found within 30 µm of injured proximal tubules compared to the groups beyond 30 µm, while changes in the B cell, T cell, and neutrophil populations were not significant (Fig. 6F, Supplementary Fig. 6). To validate the spatial transcriptomic findings, immunofluorescence microscopy was performed on DKD and control biopsies probing for LTL, IL-32, and the macrophage marker CD68 (Fig. 6G). Consistent with the prior observations, a higher density of CD68 + macrophages was seen in close proximity to IL32 + proximal tubules compared to uninjured LTL + /IL32- proximal tubules (Fig. 6G). Quantification of the percentage of CD68 + macrophages within 30 µm of LTL + and IL32 + proximal tubules was compared across four samples, and a significant increase in CD68 + macrophages was reported within 30 µm of IL32 + proximal tubules compared

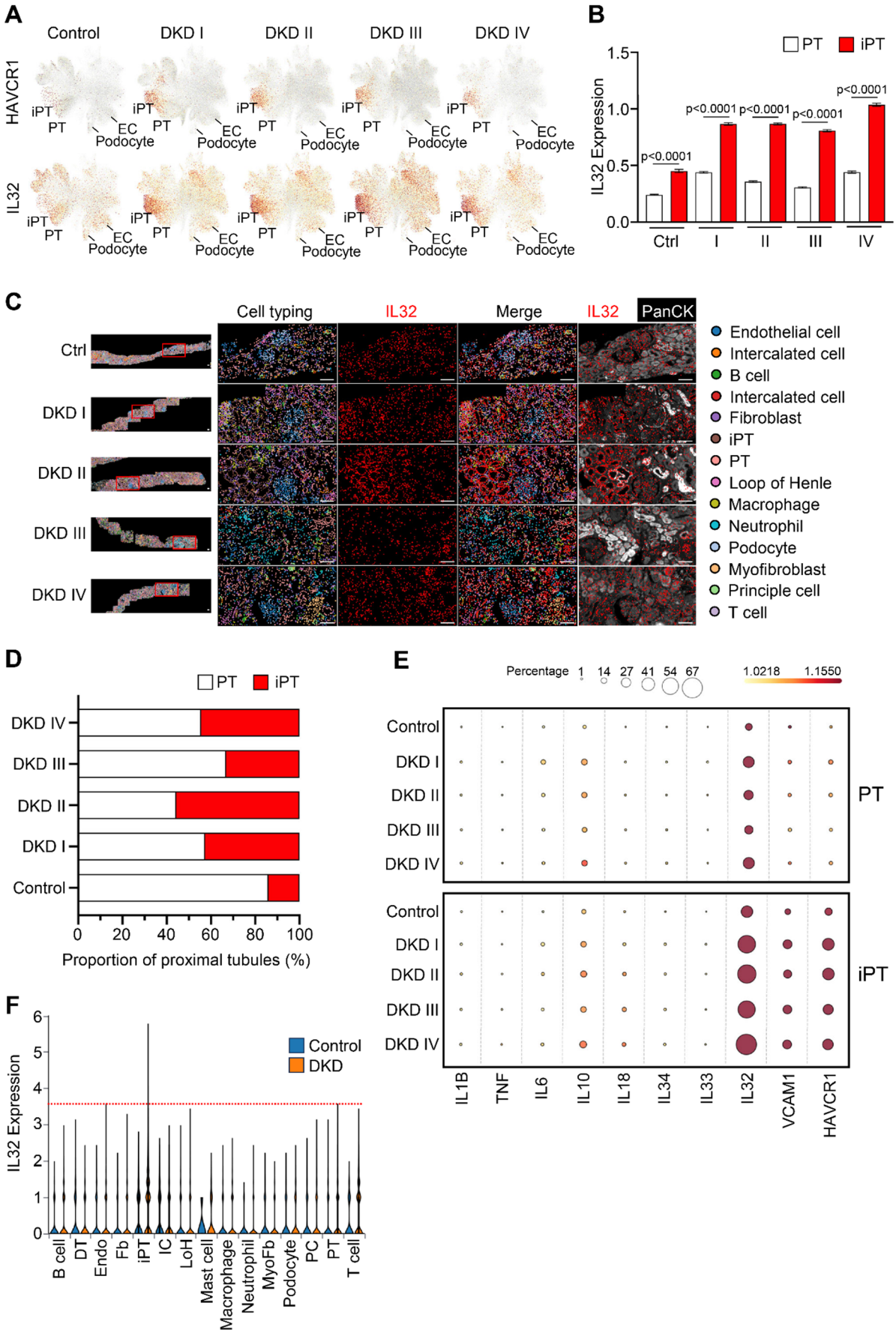
A
Control
DKD I
DKD II
DKD III
DKD IV
HAVCR1
IL32
iPT
PT
EC
Podocyte
B
PT
iPT
IL32 Expression
p<0.0001
Ctrl
I
II
III
IV
C
Cell typing
IL32
Merge
PanCK
Ctrl
DKD I
DKD II
DKD III
DKD IV
Endothelial cell
Intercalated cell
B cell
Intercalated cell
Fibroblast
iPT
PT
Loop of Henle
Macrophage
Neutrophil
Podocyte
Myofibroblast
Principle cell
T cell
D
Proportion of proximal tubules (%)
E
Percentage
1.0218
1.1550
IL1B
TNF
IL6
IL10
IL18
IL34
IL33
IL32
VCAM1
HAVCR1
F
Control
DKD
IL32 Expression
B cell
DT
Endo
Fb
iPT
IC
LoH
Mast cell
Macrophage
Neutrophil
MyoFb
Podocyte
PC
PT
T cell

Fig. 5 Injured proximal tubule populations express IL32 in diabetic kidney disease. **A** UMAP expression of HAVCR1 to mark injured proximal tubules (iPT) as well as *IL32* expression split by DKD class. Proximal tubule (PT) and endothelial cell (EC) labelled, **B** Quantification of *IL32* expression in proximal tubule (PT) and injured proximal tubule (iPT) populations split by DKD class. One way ANOVA with Kruskal-Wallis correction for multiple testing, **C** Spatial transcription of *IL32* in relation to cell typing annotation. Cell type annotation is shown in the left two panels and merge with the colour key to the right. *IL32* transcripts shown in red and overlayed with cell typing. PanCK (white) structural post staining of tissue. Scale bars represent 100 µm, **D** Changes in percentage of healthy to injured proximal tubule cells to total cell type split by DKD class. Values are percentage of total cells between the PT and iPT populations, **E** Dot plot expression of canonical DKD cytokine expression compared in injured proximal tubule cell type split by disease class, **F** IL32 expression split by cell type in control and DKD tissue samples. Distal tubule (DT), endothelial cell (Endo), fibroblast (Fb), injured proximal tubule (iPT), intercalated cell (IC), Loop of Henle (LoH), myofibroblast (MyoFb), and healthy proximal tubule (PT) labels. Red dashed line indicates the peak IL32 expression in healthy proximal tubule cells in DKD tissue used as a threshold for other cell types.

to LTL+proximal tubules (1.25% vs 0.53%, $p<0.0001$) (Fig. 6H). It is important to note that this analysis was limited to investigating the relationship in two dimensions. Taken together, this data supports the finding that macrophages preferentially co-localize to IL-32+injured proximal tubules in human DKD.

Finally, to ascertain in which phase of injury IL32 may contribute to DKD pathogenesis, kidney tissue sections were categorized into active and chronic regions within the same biopsy based on histological appearance, cell composition and *HAVCR1* expression (Fig. 7A, B). Active regions were defined by areas with less immune infiltration, as indicated by H&E/PAS staining, minimal collagen deposition, as shown by Masson trichrome staining, and *HAVCR1* expression, as determined from the single-cell digital spatial transcriptomic dataset (Fig. 7A). Chronic regions were defined by high immune cell infiltration, increased collagen deposition and tubular atrophy, low *HAVCR1* expression and an increase in fibroblast and myofibroblast cell types determined from the single-cell digital spatial transcriptomic data (Fig. 7B). Macrophages and neutrophils showed higher expression of markers *ITGAM* and *IL1B,* indicating a potential pro-inflammatory phenotype, while T cells and B cells showed higher expression of resolution/repair genes *IL10* and *TGFB1* (Fig. 7C). However, the limited gene panel constrained further immune cell subtyping. In areas of the DKD biopsies defined as active, *IL32* expression was greater compared to chronic regions and corresponded with *HAVCR1* expression (Fig. 7D). Consistent with these observations, areas defined as chronic expressed higher levels of collagen genes, *COL4A1* and *COL4A2* (Fig. 7D). Immune cell populations also differed, with active regions harboring more macrophages and neutrophils, and chronic regions containing higher numbers of T and B lymphocytes (Fig. 7E). These data suggest that IL-32 is expressed in areas of active proximal tubular cell injury and inflammation during human DKD (Fig. 8).

Discussion

Using several complementary approaches, we identify IL-32 as an intracellular, lipid-droplet associated cytokine that is highly expressed in proximal tubular cells during active injury in human DKD. Not only did IL-32 expression increase in parallel with cellular lipid droplets, but IL-32 expressing proximal tubules were in close proximity to infiltrating macrophages, suggesting that IL-32 may be an important cytokine that links lipotoxicity and renal inflammation. Collectively, these data provide a strong rationale for future mechanistic studies to dissect IL-32 function and assess its suitability as a therapeutic target in DKD.

DKD is a severe manifestation of type 1 and type 2 diabetes and the leading cause of CKD [1]. Previous research has compiled substantial support for the hypothesis that excess lipid accumulation in the kidney triggers lipotoxicity, driving DKD progression [6, 20]. In DKD, the accumulation of lipids in the tubules and the glomeruli was identified as early as 1936 by Kimmelstiel and Wilson [11]. Using a combination of conventional and advanced techniques including Nile Red spectroscopy, high resolution microscopy and spatial transcriptomics we identified IL-32 as a lipid droplet associated cytokine primarily upregulated in the proximal tubules of DKD patients. In DKD kidney patient biopsies, IL-32 expression was highest in regions of high KIM-1 expression, which is a known early marker of kidney proximal tubular injury highly expressed in early diabetic disease [30, 43]. Our findings are supported by a recent study by Wilson et al. which used single-nucleus RNA sequencing to show *IL32* expression in an injured population of *VCAM1*+proximal tubular cells in DKD biopsies [44]. *IL32* expression is highly increased in the proximal tubules of patient biopsies with active injury and inflammation, supporting our findings that *IL32* is a mediator of proximal tubular injury in DKD [45]. *IL32* was not previously reported in a transcriptome analysis of DKD of the microdissected tubular compartment of advanced DKD kidney biopsies using Affymetrix microarray assays [46]. This may be explained by the improvement of current technologies with cellular resolution, including single-cell RNA sequencing, single-nucleus RNA sequencing, and digital spatial transcriptomics, with improved sensitivity to identify previously unreported transcripts, including *IL32*. In agreement with our study, Abedini et al.'s recent study using CosMx in a DKD patient similarly found increased

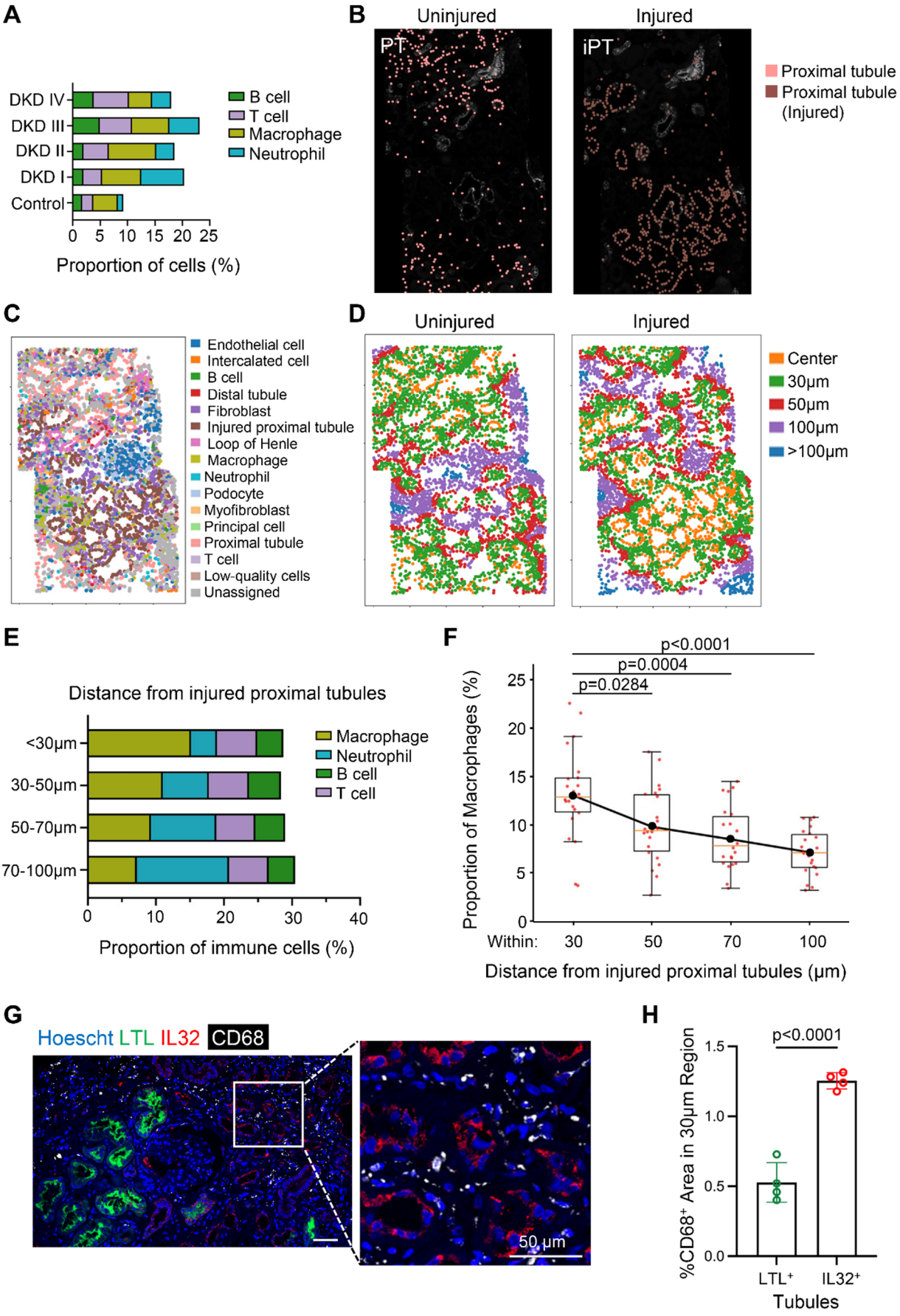
A
DKD IV
DKD III
DKD II
DKD I
Control
0 5 10 15 20 25
Proportion of cells (%)
B cell
T cell
Macrophage
Neutrophil
B
Uninjured
Injured
PT
iPT
Proximal tubule
Proximal tubule (Injured)
C
Endothelial cell
Intercalated cell
B cell
Distal tubule
Fibroblast
Injured proximal tubule
Loop of Henle
Macrophage
Neutrophil
Podocyte
Myofibroblast
Principal cell
Proximal tubule
T cell
Low-quality cells
Unassigned
D
Uninjured
Injured
Center
30µm
50µm
100µm
>100µm
E
Distance from injured proximal tubules
<30µm
30-50µm
50-70µm
70-100µm
Macrophage
Neutrophil
B cell
T cell
0 10 20 30 40
Proportion of immune cells (%)
F
p<0.0001
p=0.0004
p=0.0284
Proportion of Macrophages (%)
0 5 10 15 20 25
Within: 30 50 70 100
Distance from injured proximal tubules (µm)
G
Hoescht LTL IL32 CD68
50 µm
H
p<0.0001
%CD68+ Area in 30µm Region
0.0 0.5 1.0 1.5
LTL+ IL32+
Tubules

Fig. 6 Macrophages preferentially localize to injured proximal tubules in diabetic kidney disease tissue. **A** Changes in total immune cell type populations in different classes of DKD., **B** CosMx annotation of uninjured proximal tubule (PT) and injured PT cells, **C** Representative region of DKD class II tissue presenting both injured and uninjured proximal tubule populations, **D** Spatial proximity analysis of cells within 30 µm, 50 µm, and 100 µm of uninjured and injured proximal tubules. Distances were calculated from centroid-to-centroid, **E** Proportion of immune cells within 30 µm, 50 µm, 70 µm, and 100 µm of injured proximal tubule cells, **F** Quantification of percentage of macrophages at varying proximities to injured proximal tubules. Statistics calculated using a one-way ANOVA with Tukey's post hoc test, **G** Representative immunofluorescence imaging of diabetic kidney biopsy (class II) stained for nuclei in blue, LTL labelling for proximal tubules in green, IL32 staining in red, and CD68 macrophage staining in white. Scale bars, 50 µm, **H** Quantification of CD68+macrophage area coverage (%) within 30 um of tubules. Each point represents the average of 3 fields of view of a DKD biopsy sample (n=4). Values are mean ± SEM. CD68+area was normalized to the total area around LTL+or IL32+tubules or the entire field area. One-way ANOVA test.

IL32 expression in an injured proximal tubule cell population but did not elaborate on this finding [42].

IL-32, originally identified as natural killer cell transcript 4, was identified as a gene expressed by activated natural killer and T cells [47]. IL-32 is now recognized as a multifaceted cytokine with at least nine splice variants that exhibit distinct expression patterns and biological potency across different tissues and disease states [48, 49]. IL-32 has been implicated in numerous chronic metabolic and inflammatory conditions, including non-alcoholic fatty liver disease, atherosclerosis, chronic obstructive pulmonary disease, and rheumatoid arthritis, highlighting its potential role as a mediator and biomarker of chronic metabolic and inflammatory diseases [50–54]. Circulating IL-32 levels are elevated in patient with type 2 diabetes and are associated with an increased risk of diabetes [40]. In organoids from human primary hepatocytes, IL-32β was associated with an increase in intracellular triglyceride synthesis [55]. Sasidharan et al. recently reported that IL-32 knockdown downregulates LD in liver cells [55]. By contrast, Aass et al. reported the accumulation of LD in IL-32-depleted myeloma cells, suggesting that IL-32 may have differing roles depending on cell type [56].

Given that IL-32 localizes to both intracellular and extracellular compartments, it remains unclear whether, in proximal tubular cells, IL-32 primarily mediates autocrine or paracrine signaling, or is released into the extracellular environment. The mechanisms by which IL-32 functions in proximal tubular cells will likely be isoform specific, as distinct IL-32 isoforms may preferentially associate with lipid droplets (LDs). LD-associated IL-32 may initially act as a metabolic sensor and protective safeguard during acute inflammatory stress. However, sustained lipid dysregulation and LD accumulation may instead promote oxidative stress and tubular injury through IL-32's pro-inflammatory actions. Consistent with this model, our GeoMx spatial transcriptomics data shows that IL-32^{high} /KIM1^{high} proximal tubules from DKD patients exhibit reduced expression of lipid metabolic pathways alongside increased lipid biogenesis and oxidative stress signatures, implicating IL-32 in metabolic reprogramming and oxidative injury (Fig. 2G). Because IL-32 expression is itself induced by oxidative stress and diabetes-associated cytokines such as tumor necrosis factor-α (TNF-α) [57], these findings support the existence of a feed-forward loop in which lipid dysregulation promotes IL-32 recruitment and concentration on LDs, thereby sustaining chronic inflammation, oxidative stress and progressive tubular injury (Fig. 8). Finally, whether IL-32 is actively secreted by proximal tubular cells remains unresolved. Although IL-32 lacks a canonical signal peptide, it has been detected in the supernatant of cultured cells [53, 58, 59]. In epithelial intestinal cells, plasma cells, esophageal squamous cell carcinoma cells and astrocytes, IL-32 can be released extracellularly in response to inflammatory stimuli [60–63]. Analogous to ESSC cells and astrocytes, IL-32 may be secreted from proximal tubular cells via extracellular vesicles to communicate with infiltrating macrophages (Fig. 8). Alternatively, IL-32 may function as a damage-associated signal released from tubular cells undergoing cell death. Discriminating between these mechanisms will be an important focus of future studies.

While this study identified IL-32 as a potential marker of interest in DKD, the use of spatial transcriptomics limited its capacity to a relatively descriptive level, requiring in vitro mechanistic work in the future to elucidate the mechanism connecting IL-32 and DKD progression. Moreover, the availability of gene markers in the CosMx spatial transcriptomic dataset using the 1000-plex panel limited the scope of this study. In the near future, the entire human protein-coding transcriptome (18,933 genes) using CosMx spatial transcriptomics, which became available at the time of this submission, will enable a new depth of analysis not possible for this study [64]. Additionally, simultaneous protein coupled with transcriptome studies would unlock the ability to obtain both RNA and protein resolution [65]. These advances will also enable more robust and confident subtyping of the macrophage and immune populations.

The findings of this study highlight several important avenues for future investigation. LD-bound IL-32 may serve as an early metabolic sensor of lipid dysregulation and act as a mediator of the metabolic–inflammation axis. It remains to be determined whether intracellular IL-32 has a protective or compensatory role, or whether it contributes to promoting mitochondrial dysfunction, oxidative stress, and tubular injury through its action as a pro-inflammatory cytokine. Additionally, the identified connection between IL-32+injured proximal tubules and macrophage

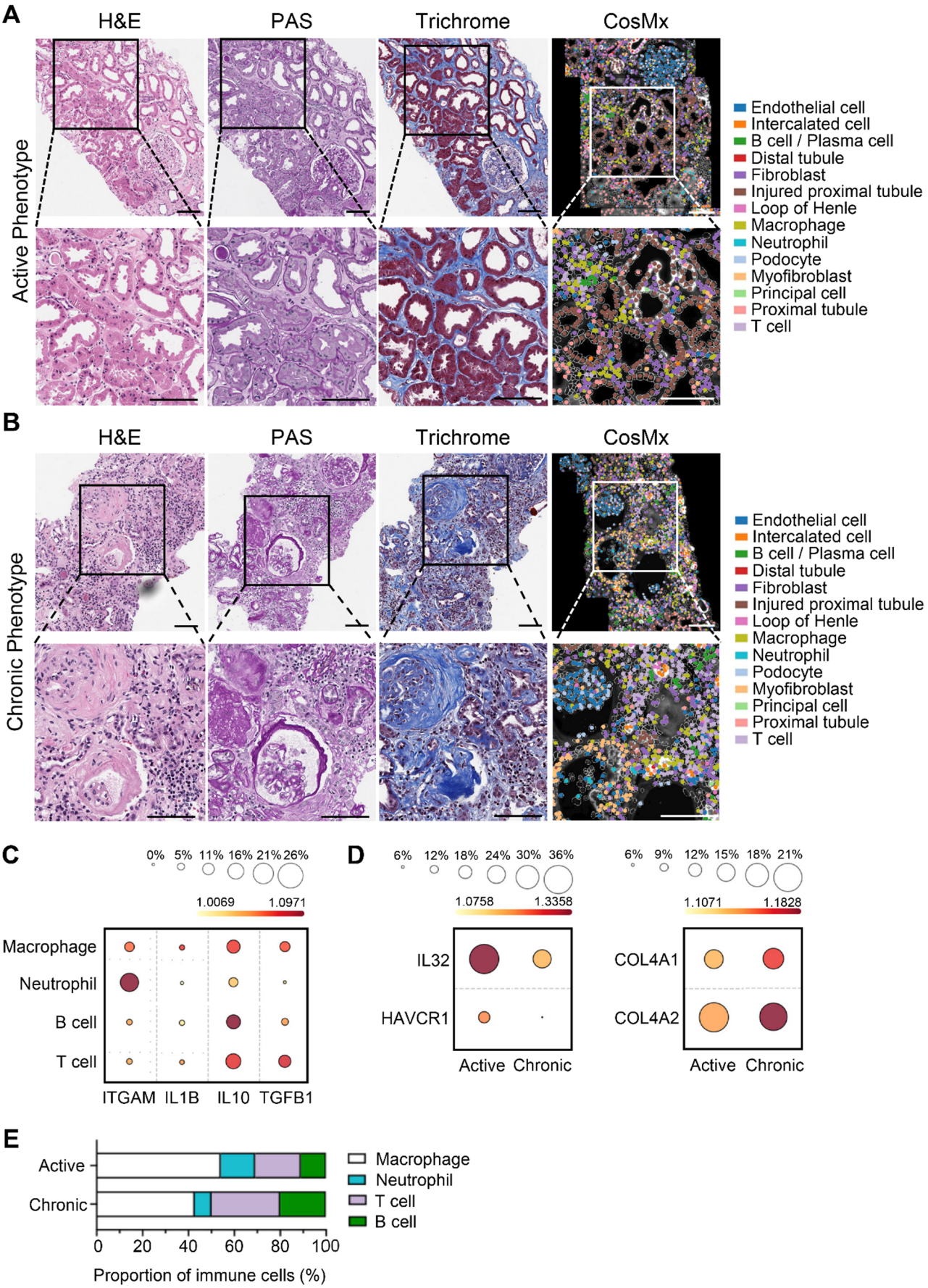
A
H&E
PAS
Trichrome
CosMx
Active Phenotype
Endothelial cell
Intercalated cell
B cell / Plasma cell
Distal tubule
Fibroblast
Injured proximal tubule
Loop of Henle
Macrophage
Neutrophil
Podocyte
Myofibroblast
Principal cell
Proximal tubule
T cell
B
H&E
PAS
Trichrome
CosMx
Chronic Phenotype
Endothelial cell
Intercalated cell
B cell / Plasma cell
Distal tubule
Fibroblast
Injured proximal tubule
Loop of Henle
Macrophage
Neutrophil
Podocyte
Myofibroblast
Principal cell
Proximal tubule
T cell
C
0% 5% 11% 16% 21% 26%
1.0069 1.0971
Macrophage
Neutrophil
B cell
T cell
ITGAM IL1B IL10 TGFB1
D
6% 12% 18% 24% 30% 36%
1.0758 1.3358
IL32
HAVCR1
Active Chronic
6% 9% 12% 15% 18% 21%
1.1071 1.1828
COL4A1
COL4A2
Active Chronic
E
Active
Chronic
0 20 40 60 80 100
Proportion of immune cells (%)
Macrophage
Neutrophil
T cell
B cell

Fig. 7 Immune population changes in proximity to active and chronic diabetic kidney injury. **A** Active phenotype diabetic kidney injury region visualized with Hematoxylin and Eosin (H&E), Periodic Acid-Schiff (PAS), and Masson Trichrome staining with CosMx cell type annotation. Scale bars, 100 µm, **B** Chronic phenotype fibrotic injury region visualized with Hematoxylin and Eosin, Periodic Acid-Schiff, and Trichrome staining with CosMx cell type annotation. Scale bars, 100 µm, **C** Dot plot expression of *ITGAM* and *IL1B* as pro-inflammatory markers as well as *IL10* and *TGFB1* as reparative markers in immune cell populations, **D** Expression of *IL32* and *HAVCR1* as markers of active injury and *COL4A1* and *COL4A2* as markers of chronic fibrotic injury compared between regions of active and chronic resident cells, **E** Change in proportion of immune cell types in areas of active and chronic phenotype injury quantified by CosMx. Values are averages of 6 regions of interest captured from 6 different DKD patient biopsies of class II and III.

cell populations raises the question of whether IL-32 plays a role in the accumulation and activation of pro-inflammatory macrophages, which are known to drive non-resolving inflammation and CKD progression [31]. IL-32 represents a potentially new biomarker and therapeutic target for human DKD, specifically targeting proximal tubular injury. An important next step will be to leverage an expanded cohort to clinically correlate tubular IL-32 expression with diabetic kidney disease progression, assessed using longitudinal measures such as estimated glomerular filtration rate and albuminuria. Future studies will be required to explore IL-32 in transgenic murine models of diabetic kidney disease [66]. While the exact molecular mechanisms by which IL-32 contributes to tubular injury and regulates lipotoxicity will require further study, we have identified IL-32 as a marker of active tubular injury in diabetic kidney disease using spatial transcriptomics and immunofluorescence. Our findings suggest the potential use of IL-32 as a biomarker for early DKD progression, with future studies required to determine if it represents a viable therapeutic target.

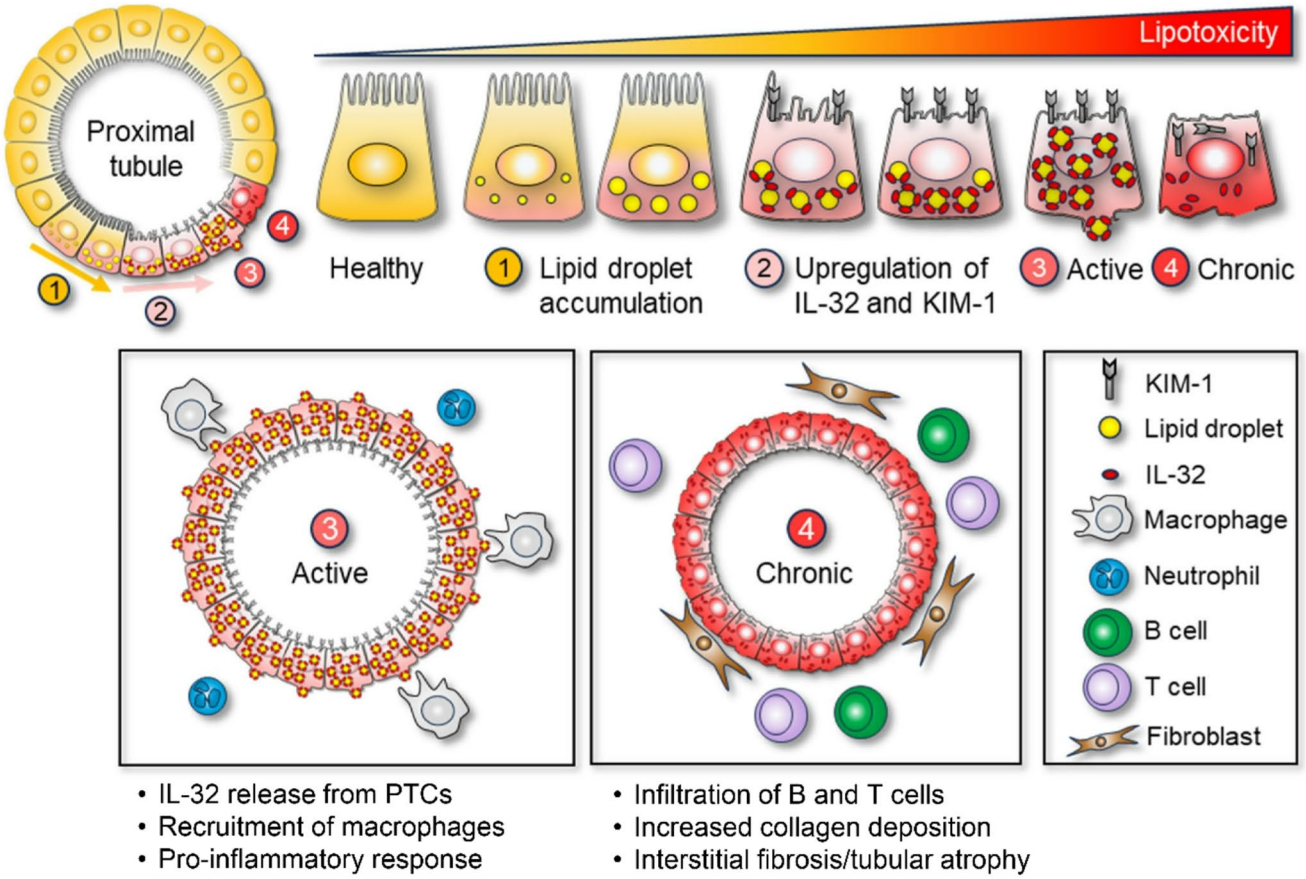

Fig. 8 Model for IL-32 mediated tubular injury and tubulointerstitial fibrosis in diabetic kidney disease (DKD). High glucose and fatty acid uptake increases intracellular free fatty acid (FFA) levels in proximal tubular cells (PTCs). Excess FFAs are intially sequestered into lipid droplets (LDs) as an adaptive response to limit lipotoxicity. While initial LD formation is protective, progressive LD accumulation leads to lipid overload and cellular stress. Importantly, LD accumulation is necessary but not sufficient for IL-32 localization. Pro-inflammatory cytokines such as TNF-α induce IL-32 expression and drives its recruitment to LDs. Elevated IL-32, in turn, amplifies TNF-α signaling, establishing a feed-forward loop that sustains chronic inflammation, lipid dysregulation, oxidative stress, tubular injury marked by kidney injury molecule 1 (KIM-1) expression and cell death. IL-32 may also be released in extracellular vesicles and taken up by infiltrating macrophages, triggering pro-inflammatory responses that contributes to chronic inflammation, collagen deposition, tubulointerstitial fibrosis and DKD progression

Supplementary Information The online version contains supplementary material available at https://doi.org/10.1007/s00011-026-02192-y.

Acknowledgements Support for infrastructure and technical was provided by the Snyder Resource Laboratories, Flow Cytometry Facility, Live Cell Imaging Facility, and the Biobank for the Molecular Classification of Kidney Disease at the Snyder Institute for Chronic Diseases, University of Calgary. The authors thank Dr. Bo-Young Ahn at the Applied Spatial Omics Centre for the expert technical assistance in running GeoMx experiments for this study. This research was supported by the NanoString CosMx SMI Technology Access Program with the team of Yan Liang, Yi Cui, Emily Killingbeck, Evelyn Metzger and Andy Nam, who provided access to the spatial molecular imager and data analysis.

Author contributions KM, HC and AI performed experiments, collected data, analyzed data and prepared figures. KM and HC contributed to the writing of the manuscript. SV, TP analyzed data and wrote the methods for the CosMx experiments. AS, WT and GA analyzed human data. HS prepared figures, analyzed and wrote methods for the GeoMx spatial transcriptomics. HB reviewed the human kidney pathology. PS supported the research with infrastructure and experimental design for Nile red staining and spectroscopy. DAM contributed to reagents, access to human tissue, data analysis and contributed to the writing of the manuscript. JC conceived the project, contributed to the experiments, analyzed the data, prepared figures and wrote the manuscript.

Funding JC was supported by a new investigator award from the Kidney Research Scientist Core Education and National Training Program (Kidney Foundation of Canada). This work was supported by operating grants from the Canadian Institutes for Health Research and infrastructure grants from the Canada Foundation for Innovation. Figure 1A and B were partially created with BioRender.com.

Declarations

Conflict of interest The authors declare that they have no competing interests.

References

1. Alicic RZ, Rooney MT, Tuttle KR. Diabetic Kidney Disease: challenges, progress, and possibilities. Clin J Am Soc Nephrol. 2017;12:2032–45.
2. Dronavalli S, Duka I, Bakris GL. The pathogenesis of diabetic nephropathy. Nat Clin Pract Endocrinol Metab. 2008;4:444–52.
3. Marshall CB. Rethinking glomerular basement membrane thickening in diabetic nephropathy: adaptive or pathogenic? Am J Physiol Renal Physiol. 2016;311:F831–43.
4. Osterby R, Gundersen HJ. Glomerular size and structure in diabetes mellitus. I. Early abnormalities. Diabetologia. 1975;11:225–9.
5. Steffes MW, Osterby R, Chavers B, Mauer SM. Mesangial expansion as a central mechanism for loss of kidney function in diabetic patients. Diabetes. 1989;38:1077–81.
6. Tervaert TW, Mooyaart AL, Amann K, Cohen AH, Cook HT, Drachenberg CB, et al. Pathologic classification of diabetic nephropathy. J Am Soc Nephrol. 2010;21:556–63.
7. Colhoun HM, Marcovecchio ML. Biomarkers of diabetic kidney disease. Diabetologia. 2018;61:996–1011.
8. Mohandes S, Doke T, Hu H, Mukhi D, Dhillon P, Susztak K. Molecular pathways that drive diabetic kidney disease. The Journal of clinical investigation 2023; 133.
9. Mitrofanova A, Fontanella AM, Merscher S, Fornoni A. Lipid deposition and metaflammation in diabetic kidney disease. Curr Opin Pharmacol. 2020;55:60–72.
10. Herman-Edelstein M, Scherzer P, Tobar A, Levi M, Gafter U. Altered renal lipid metabolism and renal lipid accumulation in human diabetic nephropathy. J Lipid Res. 2014;55:561–72.
11. Kimmelstiel P, Wilson C. Intercapillary Lesions in the Glomeruli of the Kidney. Am J Pathol. 1936;12(83–98):7.
12. Yang W, Luo Y, Yang S, Zeng M, Zhang S, Liu J, et al. Ectopic lipid accumulation: potential role in tubular injury and inflammation in diabetic kidney disease. Clin Sci (Lond). 2018;132:2407–22.
13. Moorhead JF, Chan MK, El-Nahas M, Varghese Z. Lipid nephrotoxicity in chronic progressive glomerular and tubulo-interstitial disease. Lancet. 1982;2:1309–11.
14. Mitrofanova A, Merscher S, Fornoni A. Kidney lipid dysmetabolism and lipid droplet accumulation in chronic kidney disease. Nat Rev Nephrol. 2023;19:629–45.
15. Zadoorian A, Du X, Yang H. Lipid droplet biogenesis and functions in health and disease. Nat Rev Endocrinol. 2023;19:443–59.
16. Bonventre JV, Yang L. Cellular pathophysiology of ischemic acute kidney injury. J Clin Invest. 2011;121:4210–21.
17. Kang HM, Ahn SH, Choi P, Ko YA, Han SH, Chinga F, et al. Defective fatty acid oxidation in renal tubular epithelial cells has a key role in kidney fibrosis development. Nat Med. 2015;21:37–46.
18. Petan T, Jarc E, Jusovic M. Lipid Droplets in Cancer: Guardians of Fat in a Stressful World. Molecules 2018; 23.
19. Tang C, Kanter JE, Bornfeldt KE, Leboeuf RC, Oram JF. Diabetes reduces the cholesterol exporter ABCA1 in mouse macrophages and kidneys. J Lipid Res. 2010;51:1719–28.
20. Wang Z, Jiang T, Li J, Proctor G, McManaman JL, Lucia S, et al. Regulation of renal lipid metabolism, lipid accumulation, and glomerulosclerosis in FVBdb/db mice with type 2 diabetes. Diabetes. 2005;54:2328–35.
21. Proctor G, Jiang T, Iwahashi M, Wang Z, Li J, Levi M. Regulation of renal fatty acid and cholesterol metabolism, inflammation, and fibrosis in Akita and OVE26 mice with type 1 diabetes. Diabetes. 2006;55:2502–9.
22. Mitrofanova A, Burke G, Merscher S, Fornoni A. New insights into renal lipid dysmetabolism in diabetic kidney disease. World J Diabetes. 2021;12:524–40.
23. Mitrofanova A, Mallela SK, Ducasa GM, Yoo TH, Rosenfeld-Gur E, Zelnik ID, et al. SMPDL3b modulates insulin receptor signaling in diabetic kidney disease. Nat Commun. 2019;10:2692.
24. Martinez-Garcia C, Izquierdo-Lahuerta A, Vivas Y, Velasco I, Yeo TK, Chen S, et al. Renal lipotoxicity-associated inflammation and

insulin resistance affects actin cytoskeleton organization in podocytes. PLoS ONE. 2015;10:e0142291.
25. Ducasa GM, Mitrofanova A, Mallela SK, Liu X, Molina J, Sloan A, et al. ATP-binding cassette A1 deficiency causes cardiolipin-driven mitochondrial dysfunction in podocytes. J Clin Invest. 2019;129:3387–400.
26. Falkevall A, Mehlem A, Palombo I, Heller Sahlgren B, Ebarasi L, He L, et al. Reducing VEGF-B signaling ameliorates renal lipotoxicity and protects against diabetic kidney disease. Cell Metab. 2017;25:713–26.
27. Folestad E, Mehlem A, Ning FC, Oosterveld T, Palombo I, Singh J, et al. Vascular endothelial growth factor B-mediated fatty acid flux in the adipose-kidney axis contributes to lipotoxicity in diabetic kidney disease. Kidney Int. 2025;107:492–507.
28. Merscher-Gomez S, Guzman J, Pedigo CE, Lehto M, Aguillon-Prada R, Mendez A, et al. Cyclodextrin protects podocytes in diabetic kidney disease. Diabetes. 2013;62:3817–27.
29. Wang H, Zhang S, Guo J. Lipotoxic proximal tubular injury: a primary event in diabetic kidney disease. Front Med. 2021;8:751529.
30. Mori Y, Ajay AK, Chang JH, Mou S, Zhao H, Kishi S, et al. KIM-1 mediates fatty acid uptake by renal tubular cells to promote progressive diabetic kidney disease. Cell Metab. 2021;33:1042-1061 e7.
31. Elias EE, Lau A, Belay SG, Derakhshani A, Andonegui G, Jenne CN, et al. The spleen tyrosine kinase inhibitor entospletinib resolves inflammation to promote repair following acute kidney injury. JCI Insight 2025; 10.
32. Merritt CR, Ong GT, Church SE, Barker K, Danaher P, Geiss G, et al. Multiplex digital spatial profiling of proteins and RNA in fixed tissue. Nat Biotechnol. 2020;38:586–99.
33. Vo S, Meadows K, Do H, Chapman K, Andonegui G, Muruve DA, et al. Streamlining single-cell spatial transcriptomics for human kidney tissue. Biotechniques 2025:1–14.
34. Lopez R, Regier J, Cole MB, Jordan MI, Yosef N. Deep generative modeling for single-cell transcriptomics. Nat Methods. 2018;15:1053–8.
35. McInnes L, Healy J, Melville J. UMAP: Uniform Manifold Approximation and Projection for Dimension Reduction. arXIV 2020.
36. Buitinck L, Louppe G, Blondel M, Pedregosa F, Mueller A, Grisel O, et al. API design for machine learning software: experiences from hte scikit-learn project. arXIV 2013.
37. Greenspan P, Mayer EP, Fowler SD. Nile red: a selective fluorescent stain for intracellular lipid droplets. J Cell Biol. 1985;100:965–73.
38. Kline A, Chung HJ, Rahmani W, Chun J. Semi-supervised segmentation of renal pathology: an alternative to manual segmentation and input to deep learning training. Annu Int Conf IEEE Eng Med Biol Soc. 2021;2021:2688–91.
39. Bersuker K, Peterson CWH, To M, Sahl SJ, Savikhin V, Grossman EA, et al. A proximity labeling strategy provides insights into the composition and dynamics of lipid droplet proteomes. Dev Cell. 2018;44:97-112.e7.
40. Fadaei R, Bagheri N, Heidarian E, Nouri A, Hesari Z, Moradi N, et al. Serum levels of IL-32 in patients with type 2 diabetes mellitus and its relationship with TNF-α and IL-6. Cytokine. 2020;125:154832.
41. Kirita Y, Wu H, Uchimura K, Wilson PC, Humphreys BD. Cell profiling of mouse acute kidney injury reveals conserved cellular responses to injury. Proc Natl Acad Sci U S A. 2020;117:15874–83.
42. Abedini A, Levinsohn J, Klötzer KA, Dumoulin B, Ma Z, Frederick J, et al. Single-cell multi-omic and spatial profiling of human kidneys implicates the fibrotic microenvironment in kidney disease progression. Nat Genet. 2024;56:1712–24.
43. Ichimura T, Bonventre JV, Bailly V, Wei H, Hession CA, Cate RL, et al. Kidney injury molecule-1 (KIM-1), a putative epithelial cell adhesion molecule containing a novel immunoglobulin domain, is up-regulated in renal cells after injury. J Biol Chem. 1998;273:4135–42.
44. Wilson PC, Muto Y, Wu H, Karihaloo A, Waikar SS, Humphreys BD. Multimodal single cell sequencing implicates chromatin accessibility and genetic background in diabetic kidney disease progression. Nat Commun. 2022;13:5253.
45. Lake BB, Menon R, Winfree S, Hu Q, Melo Ferreira R, Kalhor K, et al. An atlas of healthy and injured cell states and niches in the human kidney. Nature. 2023;619:585–94.
46. Woroniecka KI, Park AS, Mohtat D, Thomas DB, Pullman JM, Susztak K. Transcriptome analysis of human diabetic kidney disease. Diabetes. 2011;60:2354–69.
47. Dahl CA, Schall RP, He HL, Cairns JS. Identification of a novel gene expressed in activated natural killer cells and T cells. J Immunol. 1992;148:597–603.
48. Kang J-W, Park YS, Lee DH, Kim MS, Bak Y, Ham SY, et al. Interaction network mapping among IL-32 isoforms. Biochimie. 2014;101:248–51.
49. Choi JD, Bae SY, Hong JW, Azam T, Dinarello CA, Her E, et al. Identification of the most active interleukin-32 isoform. Immunology. 2009;126:535–42.
50. Di Benedetto P, Guggino G, Manzi G, Ruscitti P, Berardicurti O, Panzera N, et al. Interleukin-32 in systemic sclerosis, a potential new biomarker for pulmonary arterial hypertension. Arthritis Res Ther. 2020;22:127.
51. Baselli GA, Dongiovanni P, Rametta R, Meroni M, Pelusi S, Maggioni M, et al. Liver transcriptomics highlights interleukin-32 as novel NAFLD-related cytokine and candidate biomarker. 2020; 69:1855–1866.
52. Damen MSMA, Schraa K, Tweehuysen L, den Broeder AA, Netea MG, Popa CD, et al. Genetic variant in IL-32 is associated with the ex vivo cytokine production of anti-TNF treated PBMCs from rheumatoid arthritis patients. Sci Rep. 2018;8:14050.
53. Heinhuis B, Koenders MI, van de Loo FA, Netea MG, van den Berg WB, Joosten LA. Inflammation-dependent secretion and splicing of IL-32{gamma} in rheumatoid arthritis. Proc Natl Acad Sci USA. 2011;108:4962–7.
54. Damen M, Popa CD, Netea MG, Dinarello CA, Joosten LAB. Interleukin-32 in chronic inflammatory conditions is associated with a higher risk of cardiovascular diseases. Atherosclerosis. 2017;264:83–91.
55. Sasidharan K, Caddeo A, Jamialahmadi O, Noto FR, Tomasi M, Malvestiti F, et al. IL32 downregulation lowers triglycerides and type I collagen in di-lineage human primary liver organoids. Cell Rep Med. 2024;5:101352.
56. Aass KR, Mjelle R, Kastnes MH, Tryggestad SS, van den Brink LM, Aass Roseth I, et al. Intracellular IL-32 regulates mitochondrial metabolism, proliferation, and differentiation of malignant plasma cells. iScience 2022; 25:103605.
57. Aass KR, Kastnes MH, Standal T. Molecular interactions and functions of IL-32. J Leukoc Biol. 2021;109:143–59.
58. Kim SH, Han SY, Azam T, Yoon DY, Dinarello CA. Interleukin-32: a cytokine and inducer of TNFalpha. Immunity. 2005;22:131–42.
59. Wen S, Hou Y, Fu L, Xi L, Yang D, Zhao M, et al. Cancer-associated fibroblast (CAF)-derived IL32 promotes breast cancer cell invasion and metastasis via integrin β3-p38 MAPK signalling. Cancer Lett. 2019;442:320–32.
60. Sun Y, Qian Y, Chen C, Wang H, Zhou X, Zhai W, et al. Extracellular vesicle IL-32 promotes the M2 macrophage polarization and metastasis of esophageal squamous cell carcinoma via FAK/STAT3 pathway. J Exp Clin Cancer Res 2022;41:145. https://doi.org/10.1186/s13046-022-02348-8
61. Hasegawa H, Thomas HJ, Schooley K, Born TL. Native IL-32 is released from intestinal epithelial cells via a non-classical

secretory pathway as a membrane-associated protein. Cytokine. 2011;53:74–83.
62. Zahoor M, Westhrin M, Aass KR, Moen SH, Misund K, Psonka-Antonczyk KM, et al. Hypoxia promotes IL-32 expression in myeloma cells, and high expression is associated with poor survival and bone loss. Blood Adv. 2017;1:2656–66.
63. Leng K, Rooney B, McCarthy F, Xia W, Rose IVL, Bax S, et al. mTOR activation induces endolysosomal remodeling and non-classical secretion of IL-32 via exosomes in inflammatory reactive astrocytes. J Neuroinflammation 2024;21:198. https://doi.org/10.1186/s12974-024-03165-w
64. Khafizov R, Piazza E, Cui Y, Patrick M, Metzger E, McGuire D, et al. Sub-cellular Imaging of the Entire Protein-Coding Human Transcriptome (18933-plex) on FFPE Tissue Using Spatial Molecular Imaging. bioRxiv 2024:2024.11.27.625536.
65. Kulasinghe A, Kang C, Sato H, Filanoski B, Hamanishi L, Heck A, et al. Abstract 6466: discovery proteome and whole transcriptome atlas analysis of skin cancer reveals biomarkers associated with immunotherapy response and resistance. Cancer Res. 2025;85:6466–6466.
66. Gomes RS, Silva MVT, Oliveira MAP, Joosten LAB, Ribeiro-Dias F. Protective immune response mediated by neutrophils in experimental visceral leishmaniasis is enhanced by IL-32gamma. Cell Immunol. 2022;371:104449.